Kinetics and Catalysis, Vol. 44, No. 4, 2003, pp. 476–489. Translated from Kinetika i Kataliz, Vol. 44, No. 4, 2003, pp. 524–537.

Iron Catalysis of SO_2 Oxidation in the Atmosphere

A. N. Yermakov*, I. K. Larin*, A. A. Ugarov*, and A. P. Purmal'**

** Institute of Energy Problems of Chemical Physics, Russian Academy of Sciences, Moscow, 119334 Russia*

*** Semenov Institute of Chemical Physics, Russian Academy of Sciences, Moscow, 119991 Russia*

Received August 1, 2002

Abstract—The mechanisms of SO_2 oxidation catalyzed by iron ions in the droplet phase of the convective cloud in the lower atmosphere were examined. The relations of the catalytic SO_2 decrease to the concentration of the iron ions and to the intensity of fluxes to the droplet of the $OH^{\bullet}_{(g)}$ and $HO^{\bullet}_{2(g)}$ radicals were characterized. The determining role of the replacement of the low-reactive $HO^{\bullet}_{2(g)}$ ($O^{-\bullet}_{2(aq)}$) radical by the reactive $SO^{-\bullet}_{5(aq)}$ radical in the sulfite medium during daytime was revealed. This process occurred due to the coupling of the decay of the radicals and their regeneration in the liquid-phase reactions $O^{-\bullet}_{2(aq)} + FeOH^{2+}_{(aq)} \longrightarrow Fe^{2+}_{(aq)} + OH^{-}_{(aq)} + O_{2(aq)}$, $HSO^{-}_{5(aq)} + Fe^{2+}_{(aq)} \longrightarrow FeOH^{2+}_{(aq)} + SO^{-\bullet}_{4(aq)} \xrightarrow{HSO^{-}_{3(aq)},\ O_{2(aq)}} SO^{-\bullet}_{5(aq)}$.

INTRODUCTION

The nature of catalysis of sulfite[1] oxidation by transition metal ions was elucidated [1–3], and this allowed one to study these processes in the atmosphere. The interest in these processes is understandable because the scale of the anthropogenic SO_2 ejection closely approached natural emission [4]. Our previous studies [1–3] have shown that the S(IV) $\xrightarrow{Fe(II, III),\ O_{2(aq)}}$ S(VI) oxidation is a chain catalytic reaction with degenerate chain branching. Its important kinetic feature is the coupling of both the chain and catalytic channels of sulfite consumption with chain branching.[2] This coupling means the presence of two positive feedbacks in the system. Specifically, this made it possible to interpret the anomalously high catalytic activity of manganese ions in sulfite oxidation in a new way [5]. This work is devoted to the search for similar coupled processes applied to the conditions of SO_2 oxidation in cloud droplets (see [6]).

Box Model of a Convective Cloud

Several box and dynamic models of the atmosphere are known, which include blocks of liquid-phase processes [7–14] along with gas-phase reactions.[3] Proper attention has not been given so far to liquid-phase catalytic reactions in the dynamic models because of their complicated character. They are analyzed in detail in the isolated volume in the framework of simpler box models of atmospheric chemical reactions. The box model described in [12] is the most complete in this respect.[4] We propose the reduced box model of gas–liquid processes of SO_2 oxidation, which is a compromise between the degree to which their details are elaborated and the number of chemical reactions. Only the most significant processes were considered in the chemical block of the reduced model (see also [6]). It is reasonable to minimize the number of reactions taking into account other simplifications used in such models. For example, the influence of UV radiation scattering on

[1] Hereinafter sulfite is an equilibrium mixture of $SO_{2(aq)}$, $HSO^{-}_{3(aq)}$, and $SO^{2-}_{3(aq)}$, where indices (aq) denote the presence of the component in the aqueous phase, and subscript (g) denotes the gas phase.

[2] Correspondingly, $SO^{-\bullet}_{5(aq)} + HSO^{-}_{3(aq)}/SO^{2-}_{3(aq)}$, $SO^{-\bullet}_{5(aq)} + Fe^{2+}_{(aq)}$, and $HSO^{-}_{5(aq)} + Fe^{2+}_{(aq)}$.

[3] It is known that most of the SO_2 in the atmosphere is oxidized in cloud droplets [15]. For example, in the recent Great Dun Fell experiment, the measured rate of SO^{2-}_4 ion formation in the droplet phase of the orographic cloud (calculated per gas) was ≈(1–2) ppbV/h [16]. The appearance of such a cloud is related to the rise and cooling of wet air mass as the cloud moves above the area of hills, mountains, etc. When the air mass containing SO_2 moves round this cloud, no noticeable changes in the sulfur dioxide content were observed for a comparable time [6]. These studies, being a component of the broad program of the Great Dun Fell studies of atmospheric processes, are performed in the framework of the EUROTRAC (subproject Ground-Based Cloud Experiment.

[4] The CAPRAM2.3 model: 160 gas phase processes involving reactions of 12 classes of organic substances, 70 components present in the droplet phase, 34 equilibria including 31 acid–base equilibria, 6 photochemical reactions, and 199 liquid-phase chemical reactions.

0023-1584/03/4404-0476$25.00 © 2003 MAIK "Nauka/Interperiodica"

Table 1. Initial concentrations of the gas components in the reduced model

Component	Content, ppbV	Component	Content, ppbV
$SO_{2(g)}$	3	$O_{3(g)}$	32
$CH_2O_{(g)}$	0.1	$H_2O_{(g)}$	2.4×10^7
$NO_{(g)}$	10^{-2}	$CO_{(g)}$	145
$NO_{2(g)}$	2.6×10^{-2}	$CH_{4(g)}$	1660
$H_2O_{2(g)}$	1	$HNO_{3(g)}$	0.16
$OH^{\bullet}_{(g)}$	1.6×10^{-4}	$N_2O_{(g)}$	300
$HO_{2(g)}$	2.4×10^{-2}	$CH_3OOH_{(g)}$	3

Table 2. Diffusion coefficients in the gas, accommodation coefficients, and Henry constants for different atmospheric components

Component	$D_g \times 10^5$, m^2/s	α_i	$K^i_{H(298)}$, mol l^{-1} atm^{-1}	$\Delta_r H^\circ_{298}$, kJ/mol	Component	$D_g \times 10^5$, m^2/s	α_i	$K^i_{H(298)}$, mol l^{-1} atm^{-1}	$\Delta_r H^\circ_{298}$, kJ/mol
$CO_{2(g)}$	1.55	0.0002	0.0311	–20.1	$NO_{(g)}$	1.30	0.03	0.0019	–
$SO_{2(g)}$	1.28	0.035	1.24	–27.0	$NO_{2(g)}$	1.92	0.0015	0.012	–10.5
$H_2SO_{4(g)}$	1.30	0.07	2.1×10^5	–	$NO^{\bullet}_{3(g)}$	1.00	0.004	0.6	–
$O_{2(g)}$	1.00	1	0.0013	–	$N_2O_{5(g)}$	1.10	0.0037	1.4	–
$O_{3(g)}$	1.48	0.05	0.0114	–19.1	$HNO_{2(g)}$	1.30	0.5	49	–40.6
$OH^{\bullet}_{(g)}$	1.53	0.05	25	–43.9	$HNO_{3(g)}$	1.32	0.054	2.1×10^5	–72.3
$HO^{\bullet}_{2(g)}$	1.04	0.01	9.0×10^3	–	$HNO_{4(g)}$	1.30	0.1	1.0×10^5	–
$H_2O_{2(g)}$	1.46	0.11	1.02×10^5	–52.7					

Note: D_g is the diffusion coefficient, α_i is the accommodation coefficient, K^i_H is the Henry constant for the ith component, $\Delta_r H^\circ_{298}$ is the thermal effect of dissolution of the gas component (T = 298 K), and $K^i_{H(T)} = K^i_{H(298)} \exp\left(-\frac{\Delta_r H^\circ_{298}}{R}\left(\frac{1}{T} - \frac{1}{298}\right)\right)$.

the surface and inside the convective cloud on the dynamics of chemical reactions is ignored [9–14]. Turbulization at the stage of cloud formation is considered to be sufficient for smoothing the concentration gradients in the horizontal direction [11] due to which mass exchange with the surrounding gas in this direction at the cloud boundaries is neglected, etc. The reduced model is based on all these simplifications. In addition to this, as in other analogous calculations [12, 13], the cloud droplets were accepted to have the same radius r = 1 μm (10^{-6} m). For this size of droplets, the appearance of concentration gradients in them can be neglected [17, 18].[5] The volume fraction of the droplet moisture in the gas was assumed to be equal to $L = V_l/V_g = 10^{-6}$, that is, corresponding to the natural value [19].

Numerical integration of the system of stiff ordinary differential equations describing the behavior of the reduced model was performed using the Chemical Work Bench (KinTech) program package [20], which accomplished the implicit multivalued Gear method with the choice of the increment and order of the

[5] They appear due to fast liquid-phase reactions, such as $OH^{\bullet}_{(aq)}$ + $HSO^-_{3(aq)}/SO^{2-}_{3(aq)}$ (Table 3, reactions (4A) and (5A)).

scheme.[6] The time changes in the gas/droplet phase composition in the convective cloud was calculated for the equinox noon at 60° north latitude and at a height of 1 km. The initial concentrations of the components, their diffusion and accommodation coefficients, and Henry constants are presented in Tables 1 and 2.

On the Rate Constants of Atmospheric SO_2 Oxidation

Success in the simulation of the dynamics of atmospheric transformation largely determines the reliability of the rate constants of gas-liquid processes used in calculations. The rate constants of reactions (G1)–(44G) (Tables 3, 4) of $SO_{2(g)}$ consumption in the gas along with the generation and consumption of the $OH^{\bullet}_{(g)}$ and $HO^{\bullet}_{2(g)}$ radicals and other reactive gas species were taken from the JPL [21] and IUPAC [22] kinetic databases.[7] The photodissociation coefficients of individual gaseous components (Table 5, reactions (45G)–(56G)) were calculated using the Atmo program package [23]. The liquid-phase reactions, accompanying acid–base equilibria, and processes of hydrolysis and complex formation of various components of the atmosphere, which are considered in the reduced model, are presented in Tables 6–8. As can be seen (Table 6), sulfite is oxidized in droplets either in reactions (3A), (11A), (13A), and (14A), or due to the reactions involving free radicals. A substantial difference in these routes is that the final product of sulfite oxidation (sulfate ions) directly appear in reaction (3A). However, their formation in the reactions involving radicals is preceded by the formation of peroxomonosulfate.

Analysis of the known box models of the atmosphere shows that, when their chemical blocks are even excessively complete, the reliability of the kinetic parameters of the liquid-phase processes (see Tables 6–8) are doubtful in some cases. Compared to the "complete" model [12] for a series of rate constants of liquid-phase reactions, we used other, more substantiated, values. For example, in [12] the ratio of the rate constants of reactions (24A) and (23A) is presented as $k_{24A}/k_{23A} \approx 4 \times 10^{-2}$. However, according to our data [24] and results presented in [25], this ratio is equal to 7. This difference results in the $((1 + 7)/(1 + 4 \times 10^{-2}))^{1/2} \approx$ threefold difference in the rate constants of chain propagation (19A)–(22A).[8] Note that the anomalously high rate constants of these reactions ($\geq 10^8$ l mol^{-1} s^{-1}) that appeared recently [26] are unrealistic. We took into account the influence of pH on the dynamics of one of the key atmospheric reactions (6A) using the approximation $k_{6A} = k^0_{6A}[H^+_{(aq)}]$, where $k^0_{6A} = 10^7$ l mol^{-1} s^{-1} [27, 28]. The deviation of k_{6A} from this dependence found at pH ≥ 4 in [29] was ignored. In the "fast" step of $SO_{2(g)}$ consumption (see below), the contribution of the reaction considered to the consumption of sulfite is not too high and can be neglected. This contribution becomes significant at greater exposures (pH ≤ 4) when the use of the chosen approximation is completely justified. The rate constant of the $SO^{-\bullet}_{5(aq)}$ + Fe(II) reaction (34A), which is very important in the catalytic regime of sulfite oxidation, in [12] is characterized by 4.3×10^7 l mol^{-1} s^{-1} [30]. Our special experiments [31] showed that, among the values presented in the literature, 3.2×10^6 l mol^{-1} s^{-1} is valid [32]. Although the list of corrections proposed for the rate constants can be continued, we emphasize that the advantage of the reduced model is the use of more reliable kinetic characteristics and the smaller number of reactions introduced into the model. This allowed us to reveal the specificity of catalysis of sulfite oxidation by the iron ions under cloud conditions.

RESULTS AND DISCUSSION

Gas-Phase SO_2 Oxidation

The results of calculation of the rate of this process in the absence and presence of the droplet moisture

[6] For the *i*th component, the differential equations have the form

$$\frac{d[C^i_g]}{dt} = w^i_{f,g} - w^i_{c,g} - \left([C^i_g]k^i_t - [C^i_{aq}]\frac{k^i_t}{K^i_H k' T}\right)L,$$

$$\frac{d[C^i_{aq}]}{dt} = w^i_{f,aq} - w^i_{c,aq} + \left([C^i_g]k^i_t - [C^i_{aq}]\frac{k^i_t}{K^i_H k' T}\right)\frac{1}{N_A}\frac{cm^3 \times 10^3}{l},$$

where $[C^i_g]$ and $[C^i_{aq}]$ are the concentrations of the *i*th component in the gas (cm^{-3}) and in the liquid phase (mol/l), respectively; $w^i_{f,g}$ and $w^i_{c,g}$ are the overall rates of formation and consumption of the *i*th component in the gas phase reactions (cm^{-3} s^{-1}) and $w^i_{f,aq}$ and $w^i_{c,aq}$ are the rates of formation and consumption of the *i*th component in the liquid-phase reactions (mol l^{-1} s^{-1}); K^i_H is the Henry constant for the *i*th component (mol l^{-1}atm^{-1}); $k' = 1.362 \times 10^{-22}$ (atm cm^3 K^{-1}) is the Batsman constant; T is the absolute temperature (K); and N_A is Avogadro's number. According to the published data [18], we assumed that the dynamics of reversible mass exchange "gas ⇔ liquid" processes for the *i*th component is described by the sum of the inverse values of the diffusion and kinetic resistances: $k^i_t = \left[\frac{r^2}{3D_g} + \frac{4r}{3\bar{c}_i\alpha_i}\right]^{-1}$, where D_g is the diffusion coefficient in the gas (m^2/s), α_i is the dimensionless accommodation coefficient (see Table 2), and $\bar{c}_i$ is the mean thermal velocity of molecules (m/s).

[7] Hereinafter superscript $X^{\bullet}$ ($X^{-\bullet}$) denotes a radical (radical ion).

[8] The experimentally measured chain length of noncatalytic sulfite oxidation, which serves, for example, to determine the rate constant of chain propagation (19A), is proportional to $k_{19A}/(2k_{23A})^{1/2}$.

Table 3. Chemical and photochemical reactions in the gas phase

No.	Reaction	A, cm^3/s	$\frac{E_a}{R}$, K	No.	Reaction	A, cm^3/s	$\frac{E_a}{R}$, K
1G	$CH_2O_{(g)} + OH^{\bullet}_{(g)} \longrightarrow H_2O_{(g)} + HCO^{\bullet}_{(g)}$	1.0×10^{-11}	0	18G	$HNO_{3(g)} + OH^{\bullet}_{(g)} \longrightarrow NO^{\bullet}_{3(g)} + H_2O_{(g)}$	1.0×10^{-13}	0
2G	$CH_3O^{\bullet}_{(g)} + O_{2(g)} \longrightarrow CH_2O_{(g)} + HO^{\bullet}_{2(g)}$	3.9×10^{-14}	900	19G	$HNO_{4(g)} + M_{(g)} \longrightarrow HO^{\bullet}_{2(g)} + NO_{2(g)} + M_{(g)}$	2.2×10^{-21}	0
3G	$2CH_3O^{\bullet}_{2(g)} \longrightarrow 2CH_3O^{\bullet}_{(g)} + O_{2(g)}$	1.0×10^{-13}	–190	20G	$HO^{\bullet}_{2(g)} + HO^{\bullet}_{2(g)} \longrightarrow H_2O_{2(g)} + O_{2(g)}$	2.3×10^{-13}	–600
4G	$CH_3O^{\bullet}_{2(g)} + HO^{\bullet}_{2(g)} \longrightarrow CH_3OOH_{(g)} + O_{2(g)}$	3.8×10^{-13}	–800	21G	$2HO^{\bullet}_{2(g)} + M_{(g)} \longrightarrow H_2O_{2(g)} + O_{2(g)} + M_{(g)}$	1.7×10^{-33}	–1000
5G	$CH_3O^{\bullet}_{2(g)} + NO_{(g)} \longrightarrow NO_{2(g)} + CH_3O^{\bullet}_{(g)}$	3.0×10^{-12}	–280	22G	$HO^{\bullet}_{2(g)} + NO_{(g)} \longrightarrow NO_{2(g)} + OH^{\bullet}_{(g)}$	3.5×10^{-12}	–250
6G	$2CH_3O^{\bullet}_{2(g)} \longrightarrow CH_2O_{(g)} + CH_3OH_{(g)} + O_{2(g)}$	1.5×10^{-13}	–190	23G	$HO^{\bullet}_{2(g)} + O_{3(g)} \longrightarrow 2O_{2(g)} + OH^{\bullet}_{(g)}$	1.1×10^{-14}	500
7G	$CH_3OH_{(g)} + OH^{\bullet}_{(g)} \longrightarrow CH_2OH_{(g)} + H_2O_{(g)}$	6.7×10^{-12}	600	24G	$HSO^{\bullet}_{3(g)} + O_{2(g)} \longrightarrow SO_{3(g)} + HO^{\bullet}_{2(g)}$	1.3×10^{-12}	330
8G	$CH_2OH_{(g)} + O_{2(g)} \longrightarrow CH_2O_{(g)} + HO^{\bullet}_{2(g)}$	9.1×10^{-12}	0	25G	$N_2O_{(g)} + O_{(g)}{}^1D \longrightarrow 2NO_{(g)}$	6.7×10^{-11}	0
9G	$CH_{4(g)} + OH^{\bullet}_{(g)} \longrightarrow CH^{\bullet}_{3(g)} + H_2O_{(g)}$	2.5×10^{-12}	1775	26G	$N_2O_{5(g)} + M_{(g)} \longrightarrow NO_{2(g)} + NO_{3(g)} + M_{(g)}$	1.8×10^{-21}	0
10G	$CH_3OOH_{(g)} + OH^{\bullet}_{(g)} \longrightarrow H_2O_{(g)} + CH_3O^{\bullet}_{2(g)}$	2.7×10^{-12}	–200	27G	$NO_{(g)} + O_{3(g)} \longrightarrow NO_{2(g)} + O_{2(g)}$	2.0×10^{-12}	1400
11G	$CH_3OOH_{(g)} + OH^{\bullet}_{(g)} \longrightarrow H_2O_{(g)} + OH^{\bullet}_{(g)} + CH_2O_{(g)}$	1.1×10^{-12}	–200	28G	$NO_{2(g)} + O_{3(g)} \longrightarrow NO^{\bullet}_{3(g)} + O_{2(g)}$	1.2×10^{-13}	2450
12G	$H^{\bullet}_{(g)} + O_{3(g)} \longrightarrow O_{2(g)} + OH^{\bullet}_{(g)}$	1.4×10^{-10}	470	29G	$\ddot{O}_{(g)} + O_{3(g)} \longrightarrow 2O_{2(g)}$	8.0×10^{-12}	2060
13G	$H_2O_{(g)} + O_{(g)}{}^1D \longrightarrow OH^{\bullet}_{(g)} + OH^{\bullet}_{(g)}$	2.2×10^{-10}	0	30G	$O_{(g)}{}^1D + M_{(g)} \longrightarrow \ddot{O}_{(g)} + M_{(g)}$	1.8×10^{-11}	–110
14G	$H_2O_{2(g)} + \ddot{O}_{(g)} \longrightarrow HO^{\bullet}_{2(g)} + OH^{\bullet}_{(g)}$	1.4×10^{-12}	2000	31G	$OH^{\bullet}_{(g)} + CO_{(g)} \longrightarrow CO_{2(g)} + H^{\bullet}_{(g)}$	2.4×10^{-13}	0
15G	$H_2O_{2(g)} + OH^{\bullet}_{(g)} \longrightarrow H_2O_{(g)} + HO^{\bullet}_{2(g)}$	2.9×10^{-12}	160	32G	$OH^{\bullet}_{(g)} + HO^{\bullet}_{2(g)} \longrightarrow H_2O_{(g)} + O_{2(g)}$	4.8×10^{-11}	–250
16G	$HCO^{\bullet}_{(g)} + O_{2(g)} \longrightarrow CO_{(g)} + HO^{\bullet}_{2(g)}$	3.5×10^{-12}	–140	33G	$OH^{\bullet}_{(g)} + O_{3(g)} \longrightarrow O_{2(g)} + HO^{\bullet}_{2(g)}$	1.6×10^{-12}	940
17G	$HNO_{2(g)} + OH^{\bullet}_{(g)} \longrightarrow H_2O_{(g)} + NO_{2(g)}$	1.8×10^{-11}	390	34G	$2OH^{\bullet}_{(g)} \longrightarrow H_2O_{(g)} + \ddot{O}_{(g)}$	4.2×10^{-12}	240
				35G	$SO_{3(g)} + H_2O_{(g)} \longrightarrow H_2SO_{4(g)}$	1.2×10^{-15}	0

Note: A is the preexponential factor of the rate constant of the gas phase reaction. Reaction rate constants were calculated using the formula $k = A\exp(-E_a/RT)$.

Table 4. Reaction rate constants of recombination in the gas phase

No.	Reaction	Low pressures		High pressures (limit)	
		$k_{0,T} = k_{0,300}(T/300)^{-n}$*		$k_{\infty,T} = k_{\infty,300}(T/300)^{-m}$**	
		$k_{0,300}$	n	$k_{\infty,300}$	m
36G	$CH_{3(g)}^{\bullet} + O_{2(g)} + M_{(g)} \longrightarrow CH_3O_{2(g)}^{\bullet} + M_{(g)}$	4.5×10^{-31}	3.0	1.8×10^{-12}	1.7
37G	$H_{(g)}^{\bullet} + O_{2(g)} + M_{(g)} \longrightarrow HO_{2(g)}^{\bullet} + M_{(g)}$	5.7×10^{-32}	1.6	7.5×10^{-11}	0
38G	$NO_{2(g)} + HO_{2(g)}^{\bullet} + M_{(g)} \longrightarrow HNO_{4(g)} + M_{(g)}$	1.8×10^{-31}	3.2	4.7×10^{-12}	1.4
39G	$NO_{2(g)} + OH_{(g)}^{\bullet} + M_{(g)} \longrightarrow HNO_{3(g)} + M_{(g)}$	2.5×10^{-30}	4.4	1.6×10^{-11}	1.7
40G	$NO_{3(g)}^{\bullet} + NO_{2(g)} + M_{(g)} \longrightarrow N_2O_{5(g)} + M_{(g)}$	2.2×10^{-30}	3.9	1.5×10^{-12}	0.7
41G	$\ddot{O}_{(g)} + O_{2(g)} + M_{(g)} \longrightarrow O_{3(g)} + M_{(g)}$	6.0×10^{-34}	2.3	–	–
42G	$OH_{(g)}^{\bullet} + NO_{(g)} + M_{(g)} \longrightarrow HNO_{2(g)} + M_{(g)}$	7.0×10^{-31}	2.6	3.6×10^{-11}	0.1
43G	$OH_{(g)}^{\bullet} + OH_{(g)}^{\bullet} + M_{(g)} \longrightarrow H_2O_{2(g)} + M_{(g)}$	6.2×10^{-31}	1.0	2.6×10^{-11}	0
44G	$SO_{2(g)} + OH_{(g)}^{\bullet} + M \longrightarrow HSO_{3(g)}^{\bullet} + M$	3.0×10^{-31}	3.3	1.5×10^{-12}	0

Note: (1) Dimensionalities of constants * cm^6/s, ** cm^3/s.

(2) Rate constant of the trimolecular reaction in the transition region of pressures was calculated using the formula $k_T(M) = \left(\frac{k_{0,T}[M]}{1 + (k_{0,T}[M]/k_{\infty,T})}\right)^{0.6\{1 + [\log_{10}(k_{0,T}[M]/k_{\infty,T})]^2\}^{-1}}$, where [M] is the concentration of molecules, and T is temperature.

Table 5. Photodissociation processes in the gas phase

No.	Process	J, s^{-1}	No.	Process	J, s^{-1}
45G	$O_{3(g)} \longrightarrow O_{(g)}{}^1D + O_{2(g)}$	1.7×10^{-5}	51G	$CH_2O_{(g)} \longrightarrow HCO_{(g)}^{\bullet} + H_{(g)}^{\bullet}$	2.0×10^{-5}
46G	$NO_{2(g)} \longrightarrow NO_{(g)} + \ddot{O}_{(g)}$	9.3×10^{-3}	52G	$H_2O_{2(g)} \longrightarrow OH_{(g)}^{\bullet} + OH_{(g)}^{\bullet}$	5.6×10^{-6}
47G	$O_{3(g)} \longrightarrow \ddot{O}_{(g)} + O_{2(g)}$	3.4×10^{-4}	53G	$HNO_{2(g)} \longrightarrow OH_{(g)}^{\bullet} + NO_{(g)}$	1.7×10^{-3}
48G	$CH_2O_{(g)} \longrightarrow H_{2(g)} + CO_{(g)}$	3.8×10^{-5}	54G	$NO_{3(g)}^{\bullet} \longrightarrow NO_{2(g)} + \ddot{O}_{(g)}$	0.16
49G	$NO_{3(g)}^{\bullet} \longrightarrow NO_{(g)} + O_{2(g)}$	1.9×10^{-2}	55G	$CH_3OOH_{(g)} \longrightarrow OH_{(g)}^{\bullet} + CH_3O_{(g)}^{\bullet}$	4.05×10^{-6}
50G	$HNO_{3(g)} \longrightarrow NO_{2(g)} + OH_{(g)}^{\bullet}$	2.7×10^{-7}	56G	$HNO_{4(g)} \longrightarrow HO_{2(g)}^{\bullet} + NO_{2(g)}$	2.4×10^{-6}

Note: J is the photodissociation coefficient, s^{-1}.

show that the reduced model data are in agreement with the known data for other models. The figure shows that the initial content of sulfur dioxide only changes by ~4% in 10^4 s, which exceeds the characteristic lifetime of the cloud (≈1 h [19]). Such a low rate of sulfur dioxide conversion is explained by the low concentration of $OH_{(g)}^{\bullet}$ radicals, which is the main "cleaner" of the atmosphere [33]. According to our calculations, in the daytime the concentration of these species is $[OH_{(g)}^{\bullet}] \approx 4 \times 10^6$ cm^{-3}. Therefore, the rate of the SO_2 decrease (w) in the reaction with the $OH_{(g)}^{\bullet}$ radicals (44G) is $w \approx w_{44G} = k_{44G}[OH_{(g)}^{\bullet}][SO_{2(g)}] \approx 3 \times 10^5$ cm^{-3} s^{-1} (~0.04 ppbV/h). The $[OH_{(g)}^{\bullet}]$ value in this estimate is only ~30% lower than that presented in the more "complete" model [13].

The concentration of the $HO^{\bullet}_{2(g)}$ radical and other active species are in satisfactory agreement with the calculations in [13] and other works. For example, in our case, $[HO^{\bullet}_{2(g)}] \sim 5 \times 10^8$ and in the cited calculations, $[HO^{\bullet}_{2(g)}] \sim 5.8 \times 10^8$ cm^{-3}. Almost the same $[HO^{\bullet}_{2(g)}]$ value is presented in [12]. A good agreement is observed when the rates of generation of the $OH^{\bullet}_{(g)}$ radicals are compared. This rate is $\sim 6 \times 10^6$ in our calculations, $\sim 10^7$ according to [12], and $\sim 7 \times 10^6$ cm^{-3} s^{-1} according to [13]. The agreement is achieved when the rates of conversion of the $OH^{\bullet}_{(g)}$ and $HO^{\bullet}_{2(g)}$ radicals into each other are compared. For example, according to [13], the sum $(w_{22G} + w_{23G}) = 1.9 \times 10^6$ cm^{-3} s^{-1}, and in our calculation it is $\approx 1.5 \times 10^6$ cm^{-3} s^{-1}. Such a small difference with the complete models demonstrates that the reduced model can be used to describe gas-phase reactions. Note that the reduced model ignored the reactions of $OH^{\bullet}_{(aq)}$ with alcohols, aldehydes, ketones, and other numerous organic components of the atmosphere [34]. The agreement of the $[OH^{\bullet}_{(g)}]$ values obtained in the reduced model and in the complete models is determined by the fact that, in both cases, the main sink of $OH^{\bullet}_{(g)}$ is its interaction with CO and CH_4 ((9G) and (31G)).

Reactions in the Two-Phase System

In the presence of droplet moisture, the self-purification of the atmosphere from $SO_{2(g)}$ is sharply intensified (see figure), and two steps of its consumption are observed. The first, faster step ($\Delta[SO_{2(g)}] \approx 1$ ppbV) ceases for $\leq 2 \times 10^3$ s. The rate of the SO_2 decrease for this time interval compared to the gas phase transformations increases $\geq 10^2$ times! As calculations show, this decrease in $SO_{2(g)}$ occurs mainly due to the $HSO^-_{3(aq)} + H_2O_{2(aq)} + H^+$ reaction (3A) in the droplet phase. The contribution of the reactions involving ozone and radicals to sulfite consumption in the first step does not exceed 25%. The jump in the decrease in the SO_2 content in the gas during this period decreases the pH of the droplets from 5.6 to $\approx$pH 4 ($\Delta[H^+] \approx 2P_{H_2O_2}/R'TL \approx 8 \times 10^{-5}$ mol/l (see reaction (3A)), where $P_{H_2O_2}$ is the partial pressure of $H_2O_{2(g)}$ (atm) and R' is the gas constant (l atm mol^{-1} K^{-1}). This pH decrease results in a decrease in the solubility[9] of SO_2, $[S(IV)]_{t > 2 \times 10^3} \approx [HSO^-_{3(aq)}] \approx K_{13E}[H_2O]_l K_H^{SO_2}(P_{SO_2} - P_{H_2O_2})/\Delta[H^+_{aq}] \approx 3.8 \times 10^{-7}$ mol/l. (At the initial moment, $[HSO_3^-]_{t \approx 0} \approx (K_{13E}[H_2O]_l K_H^{SO_2} P_{SO_2})^{1/2} \approx 8 \times 10^{-6}$ mol/l.) Some, although lower, contribution to a decrease in the pH (and the decrease in the solubility of SO_2) during the same time period is made by the dissolution of "acidic" components in the droplets: $H_2SO_{4(g)}$, $HNO_{3(g)}$, $SO_{2(g)}$, $HNO_{2(g)}$, $HNO_{4(g)}$, $N_2O_{5(g)}$, etc.

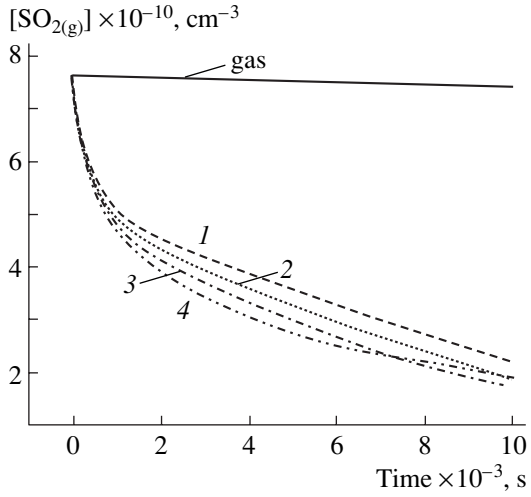

Changes in the sulfur dioxide content in the gas for different scenarios calculated within the framework of the reduced model (see text). $[Fe]_0 \times 10^{-7}$, mol/l: (*2*) 1, (*3*) 2, and (*4*) 4; (*1*) gas + droplets.

Now let us consider the influence of the liquid-phase processes on the concentrations of $OH^{\bullet}_{(g)}$ and $HO^{\bullet}_{2(g)}$. The concentration of the hydroxyl radicals in the presence of droplet moisture changes insignificantly: $\Delta[OH^{\bullet}_{(g)}] = [OH^{\bullet}_{(g)}] - [OH^{\bullet}_{(g)}]_l \approx 1.2 \times 10^6$ cm^{-3} ($\leq$30% of $[OH^{\bullet}_{(g)}]$), where $[OH^{\bullet}_{(g)}]_l$ is the concentration of $OH^{\bullet}$ radicals in the gas phase in the presence of droplets. A similar decrease in $[OH^{\bullet}_{(g)}]$ calculated in [13] in the absence of SO_2 in the gas was related to the liquid-phase reaction $OH^{\bullet}_{(aq)} + CH_2(OH)_{2(aq)}$. Taking into account this process ($[CH_2O_{(g)}] = 0.1$ ppbV) within the framework of the reduced model resulted in the additional decrease in $[OH^{\bullet}_{(g)}]_l$ ($\Delta[OH^{\bullet}_{(g)}]_l \approx 1 \times 10^6$ cm^{-3}). The ratio $[HO^{\bullet}_{2(g)}]/[HO^{\bullet}_{2(g)}]_l \approx 24$, which was calculated in [13] is close to our value (~30). Such a decrease in their concentration is attributed to the dissolution of $HO^{\bullet}_{2(g)}$ ($K_H^{HO^{\bullet}_2} = 9 \times 10^3$ mol l^{-1} atm^{-1} [13])[10] and subsequent liquid-phase reactions $HO^{\bullet}_{2(aq)} + HO^{\bullet}_{2(aq)}/O^{-\bullet}_{2(aq)}$ (1A), (2A) and $SO^{-\bullet}_{5(aq)} + HO^{\bullet}_{2(aq)}/O^{-\bullet}_{2(aq)}$ (17A), (18A). When ignoring these chemical transformations, a decrease in $[HO^{\bullet}_{2(aq)}]_l$ would be only 20% [19]. Reac-

[9] In this and further estimates, the time interval 2×10^3–4×10^3 s is considered.

[10] The value $K_H^{HO^{\bullet}_2} = 2 \times 10^3$ mol l^{-1}atm^{-1} was used in the calculations in [13].

Table 6. Chemical and photochemical reactions in the droplet moisture

No.	Reaction	k_{iA}, l mol^{-1} s^{-1}	No.	Reaction	k_{iA}, l mol^{-1} s^{-1}
1A	$HO^{\bullet}_{2(aq)} + HO^{\bullet}_{2(aq)} \longrightarrow H_2O_{2(aq)} + O_{2(aq)}$	8.3×10^5	19A	$SO^{-\bullet}_{5(aq)} + HSO^{-}_{3(aq)} \longrightarrow SO^{2-}_{4(aq)} + SO^{-\bullet}_{4(aq)} + H^{+}_{(aq)}$	2.0×10^2
2A	$HO^{\bullet}_{2(aq)} + O^{-\bullet}_{2(aq)} \xrightarrow{H_2O} H_2O_{2(aq)} + O_{2(aq)} + OH^{-}_{(aq)}$	9.7×10^7	20A	$SO^{-\bullet}_{5(aq)} + HSO^{-}_{3(aq)} \longrightarrow HSO^{-}_{5(aq)} + SO^{-\bullet}_{3(aq)}$	3.4×10^3
3A*	$HSO^{-}_{3(aq)} + H_2O_{2(aq)} + H^{+}_{(aq)} \longrightarrow SO^{2-}_{4(aq)} + H_2O + 2H^{+}_{(aq)}$	6.9×10^7	21A	$SO^{-\bullet}_{5(aq)} + SO^{2-}_{3(aq)} \longrightarrow SO^{-\bullet}_{4(aq)} + SO^{2-}_{4(aq)}$	5.5×10^5
4A	$SO^{2-}_{3(aq)} + OH^{\bullet}_{(aq)} \longrightarrow OH^{-}_{(aq)} + SO^{-\bullet}_{3(aq)}$	4.6×10^9	22A	$SO^{-\bullet}_{5(aq)} + SO^{2-}_{3(aq)} \longrightarrow SO^{2-}_{5(aq)} + SO^{-\bullet}_{3(aq)}$	2.1×10^5
5A	$HSO^{-}_{3(aq)} + OH^{\bullet}_{(aq)} \longrightarrow H_2O + SO^{-\bullet}_{3(aq)}$	2.7×10^9	23A	$SO^{-\bullet}_{5(aq)} + SO^{-\bullet}_{5(aq)} \longrightarrow S_2O^{2-}_{8(aq)} + O_{2(aq)}$	1.3×10^7
6A*	$HSO^{-}_{5(aq)} + HSO^{-}_{3(aq)} + H^{+}_{(aq)} \longrightarrow 2SO^{2-}_{4(aq)} + 3H^{+}_{(aq)}$	1.0×10^7	24A	$SO^{-\bullet}_{5(aq)} + SO^{-\bullet}_{5(aq)} \longrightarrow 2SO^{-\bullet}_{4(aq)} + O_{2(aq)}$	8.7×10^7
7A	$N_2O_{5(aq)} + H_2O \longrightarrow 2H^{+}_{(aq)} + 2NO^{-}_{3(aq)}$	5.0×10^9	25A	$FeOH^{2+}_{(aq)} + HO^{\bullet}_{2(aq)} \longrightarrow Fe^{2+}_{(aq)} + O_{2(aq)} + H_2O$	1.3×10^5
8A	$NO^{\bullet}_{3(aq)} + HSO^{-}_{3(aq)} \longrightarrow NO^{-}_{3(aq)} + SO^{-\bullet}_{3(aq)} + H^{+}_{(aq)}$	1.3×10^9	26A	$FeOH^{2+}_{(aq)} + O^{-\bullet}_{2(aq)} \longrightarrow Fe^{2+}_{(aq)} + OH^{-}_{(aq)} + O_{2(aq)}$	1.5×10^8
9A	$NO^{\bullet}_{3(aq)} + SO^{2-}_{3(aq)} \longrightarrow NO^{-}_{3(aq)} + SO^{-\bullet}_{3(aq)}$	3.0×10^8	27A	$Fe(OH)^{+}_{2(aq)} + O^{-\bullet}_{2(aq)} \longrightarrow Fe^{2+}_{(aq)} + 2OH^{-}_{(aq)} + O_{2(aq)}$	1.5×10^8
10A	$O^{-\bullet}_{2(aq)} + O_{3(aq)} \xrightarrow{H^+} 2O_{2(aq)} + OH^{\bullet}_{(aq)}$	1.5×10^9	28A	$Fe^{2+}_{(aq)} + H_2O_{2(aq)} \longrightarrow OH^{\bullet}_{(aq)} + OH^{-}_{(aq)} + Fe^{3+}_{(aq)}$	76
11A	$SO_2 + O_{3(aq)} \xrightarrow{H_2O} HSO^{-}_{4(aq)} + O_{2(aq)} + H^{+}_{(aq)}$	2.4×10^4	29A	$Fe^{2+}_{(aq)} + S_2O^{2-}_{8(aq)} \longrightarrow Fe^{3+}_{(aq)} + SO^{2-}_{4(aq)} + SO^{-\bullet}_{4(aq)}$	12
12A	$SO^{-\bullet}_{3(aq)} + O_{2(aq)} \longrightarrow SO^{-\bullet}_{5(aq)}$	2.5×10^9	30A	$Fe^{2+}_{(aq)} + HSO^{-}_{5(aq)} \longrightarrow Fe^{3+}_{(aq)} + SO^{-\bullet}_{4(aq)} + OH^{-}_{(aq)}$	3.0×10^4
13A	$SO^{2-}_{3(aq)} + O_{3(aq)} \longrightarrow SO^{2-}_{4(aq)} + O_{2(aq)}$	1.5×10^9	31A	$Fe^{2+}_{(aq)} + O^{-\bullet}_{2(aq)} \xrightarrow{2H^+} H_2O_{2(aq)} + Fe^{3+}_{(aq)}$	1.0×10^7
14A	$HSO^{-}_{3(aq)} + O_{3(aq)} \longrightarrow HSO^{-}_{4(aq)} + O_{2(aq)}$	3.7×10^5	32A	$Fe^{2+}_{(aq)} + HO^{\bullet}_{2(aq)} \longrightarrow Fe^{3+}_{(aq)} + HO^{-}_{2(aq)}$	1.2×10^6
15A	$SO^{-\bullet}_{4(aq)} + HSO^{-}_{3(aq)} \longrightarrow HSO^{-}_{4(aq)} + SO^{-\bullet}_{3(aq)}$	3.2×10^8	33A	$Fe^{2+}_{(aq)} + SO^{-\bullet}_{4(aq)} \longrightarrow Fe^{3+}_{(aq)} + SO^{2-}_{4(aq)}$	3.0×10^8
16A	$SO^{-\bullet}_{4(aq)} + SO^{2-}_{3(aq)} \longrightarrow SO^{2-}_{4(aq)} + SO^{-\bullet}_{3(aq)}$	3.2×10^8	34A	$Fe^{2+}_{(aq)} + SO^{-\bullet}_{5(aq)} \longrightarrow Fe^{3+}_{(aq)} + SO^{2-}_{5(aq)}$	3.2×10^6
17A	$SO^{-\bullet}_{5(aq)} + HO^{\bullet}_{2(aq)} \longrightarrow HSO^{-}_{5(aq)} + O_{2(aq)}$	1.7×10^9	35A**	$FeOHSO_3H^{+} \longrightarrow Fe^{2+}_{(aq)} + H_2O + SO^{-\bullet}_{5(aq)}$	0.2
18A	$SO^{-\bullet}_{5(aq)} + O^{-\bullet}_{2(aq)} \longrightarrow SO^{2-}_{5(aq)} + O_{2(aq)}$	1.7×10^9			

*The rate constant has dimensionality l^2 mol^{-2} s^{-1}.
**The rate constant has dimensionality s^{-1}.

Table 7. Photodissociation reactions in the liquid phase

No.	Reaction	J, s^{-1}	No.	Reaction	J, s^{-1}
36A	$NO^-_{2(aq)} \xrightarrow{H_2O} NO_{(aq)} + OH^{\bullet}_{(aq)} + OH^-_{(aq)}$	2.6×10^{-5}	39A	$FeOH^{2+}_{(aq)} \longrightarrow Fe^{2+}_{(aq)} + OH^{\bullet}_{(aq)}$	4.5×10^{-3}
37A	$H_2O_{2(aq)} \longrightarrow 2OH^{\bullet}_{(aq)}$	7.2×10^{-6}	40A	$Fe(OH)^+_{2(aq)} \longrightarrow Fe^{2+}_{(aq)} + OH^{\bullet}_{(aq)} + OH^-_{(aq)}$	5.8×10^{-3}
38A	$NO^-_{3(aq)} \xrightarrow{H_2O} NO_{2(aq)} + OH^{\bullet}_{(aq)} + OH^-_{(aq)}$	5.6×10^{-5}	41A	$FeSO^+_{4(aq)} \longrightarrow Fe^{2+}_{(aq)} + SO^{-\bullet}_{4(aq)}$	6.4×10^{-3}

Note: J is the photodissociation coefficient.

tions (1A), (2A), (17A), and (18A) leading to the formation of $H_2O_{2(aq)}$ and $HSO^-_{5(aq)}$ are the reason for the "slow" step of the $SO_{2(g)}$ decrease (see figure).

The cessation of the fast step corresponds to the almost complete consumption of $H_2O_{2(g)}$ (1 ppbV). However, reaction (3A) continues to play the role of the main reaction of sulfite oxidation ($w_{3A}/w_{6A} \approx 3$) in the slow step of the $SO_{2(g)}$ decrease. The formation of $H_2O_{2(aq)}$ due to the recombination of $HO^{\bullet}_{2(aq)}/O^{-\bullet}_{2(aq)}$ instead of its absorption by droplets is the source of $H_2O_{2(aq)}$ in this period. The value of the difference in the rates of formation of hydrogen peroxide in the gas and droplets during the recombination of the $HO^{\bullet}_{2(g)}$ radicals for the slow step can be shown. In the gas $w_{20G} \approx 1 \times 10^3$ cm^{-3} s^{-1}, and in the liquid (calculated per gas) as a result of reactions (1A) and (2A), $w_{1A} + w_{2A} \approx 8 \times 10^5$ cm^{-3} s^{-1}. The pH of the droplet phase slowly decreases in parallel with a decrease in $SO_{2(g)}$ via the "slow" mechanism. The pH value of the droplet phase (close to limiting and corresponding to ~80% conversion of SO_2 in the gas) is ~3.9.

Computer simulations of the fluxes to the droplet of the $OH^{\bullet}$ and $HO^{\bullet}_2$ radicals for the slow step of $SO_{2(g)}$ consumption give $W_{OH^{\bullet}} \approx 1.3 \times 10^6$ and $W_{HO^{\bullet}_2} \approx 3.7 \times 10^6$ cm^{-3} s^{-1}. The cross recombination of the $SO^{-\bullet}_{5(aq)}$ radicals with $HO^{\bullet}_{2(aq)}/O^{-\bullet}_{2(aq)}$ in the liquid phase is thus responsible for the ≤30% decrease in $[HO^{\bullet}_{2(g)}]_l$. The rate of the slow step of the $SO_{2(g)}$ decrease (see figure) is determined by the rate of accumulation of $H_2O_{2(aq)}$ and $HSO^-_{5(aq)}$ in the droplet moisture. The averaged rate of sulfite consumption expressed via the fluxes to the droplet of the $OH^{\bullet}_{(g)}$ and $HO^{\bullet}_{2(g)}$ radicals is $\bar{w} \approx k_{3A}[H_2O_{2(aq)}][HSO^-_{3(aq)}] + 2k_{6A}[HSO^-_{5(aq)}] \times [HSO^-_{3(aq)}] \approx (W_{HO^{\bullet}_2} - W_{OH^{\bullet}}/2 + 2W_{OH^{\bullet}} = W_{HO^{\bullet}_2}/2 + 1.5w_{5A} \approx 3.3 \times 10^6$ cm^{-3} s^{-1} (≈ 0.47 ppbV/h). The difference (in parentheses) between the fluxes to the droplet of the $HO^{\bullet}_{2(g)}$ and $OH^{\bullet}_{(g)}$ radicals is the contribution to the consumption of the $SO^{-\bullet}_{5(aq)}$ radicals from recombination reactions (17A) and (18A) ($W_{HO^{\bullet}_2}/W_{OH^{\bullet}} \approx 3$). The numerical coefficients reflect the stoichiometry of $HSO^-_{3(aq)}$ oxidation in the reactions with $H_2O_{2(aq)}$ and with $HSO^-_{5(aq)}$. This estimate is close to the result obtained by computer simulations ($\bar{w} \approx 0.5$ ppbV/h). Thus, liquid-phase reactions involving free radicals play the key role in the self-purification of the atmosphere from SO_2 in the presence of the droplet moisture. These reactions remove up to ~70% sulfur dioxide from the gas.

Influence of Iron Ions

Iron is the most abundant metal in the atmosphere. Its content in the cloud droplets varies from 5×10^{-8} in a sea atmosphere to 10^{-4} mol/l in an urbanized atmosphere (0.001–5 μg/m^3) [35]. Iron exists in the droplets as a microcolloid along with its dissolved forms. According to the data in [36], only ~30% iron found in rain droplets exists in ionic form. This conclusion follows from the measurement of its total content and the content in the filtrate of the rain moisture. The catalytic effect of the iron microcolloid on sulfite oxidation was not studied.[11] It is only known that the addition of soot particles containing inclusions of similar iron compounds to a sulfite solution results in the consumption of S(IV) most likely due to the transition of some portion of the microcolloid to the soluble form [37]. The redox dissolution of iron(III) hydroxide occurs in a

[11] Our simulations of the pH dependence of the apparent rate constant of sulfite oxidation catalyzed by the iron ions in the approximation of zero activity of this microcolloid gave values that agree with the experiment. This gives indirect evidence for the low catalytic activity of the $Fe(OH)_{3(aq)}$ microcolloid toward sulfite oxidation.

Table 8. Dissociation equilibria in the droplet moisture

No.	Equilibrium	K_i	Direct		Inverse	
			$\vec{A}_{298}$, $\frac{l^{-(n-1)}}{mol^{-(n-1)}\,s}$	$\frac{\vec{E}_a}{R}$, K	$\overleftarrow{A}_{298}$, $\frac{l^{-(n-1)}}{mol^{-(n-1)}\,s}$	$\frac{\overleftarrow{E}_a}{R}$, K
1E	$CO_{2(aq)} + H_2O \longleftrightarrow H_2CO_{3(aq)}$	7.7×10^{-7}	4.3×10^{-2}	9250	5.6×10^{4}	8500
2E	$H_2CO_{3(aq)} \longleftrightarrow H^+_{(aq)} + HCO^-_{3(aq)}$	4.3×10^{-7}	2.15×10^{4}	–	5×10^{10}	–
3E	$H_2O \longleftrightarrow H^+_{(aq)} + OH^-_{(aq)}$	1.8×10^{-16}	2.34×10^{-5}	6800	1.3×10^{11}	–
4E	$H_2SO_{4(aq)} \longleftrightarrow HSO^-_{4(aq)} + H^+_{(aq)}$	1.0×10^{2}	5.0×10^{12}	–	5×10^{10}	–
5E	$HCO^-_{3(aq)} \longleftrightarrow H^+_{(aq)} + CO^{2-}_{3(aq)}$	4.69×10^{-11}	2.35	1820	5×10^{10}	–
6E	$HNO_{2(aq)} \longleftrightarrow H^+_{(aq)} + NO^-_{2(aq)}$	5.3×10^{-4}	2.65×10^{7}	1760	5×10^{10}	–
7E	$HNO_{3(aq)} \longleftrightarrow H^+_{(aq)} + NO^-_{3(aq)}$	22	1.1×10^{12}	–1800	5×10^{10}	–
8E	$HNO_{4(aq)} \longleftrightarrow H^+_{(aq)} + NO^-_{4(aq)}$	1.0×10^{-5}	5.0×10^{5}	–	5×10^{10}	–
9E	$HO^{\bullet}_{2(aq)} \longleftrightarrow O^{-\bullet}_{2(aq)} + H^+_{(aq)}$	1.6×10^{-5}	8.0×10^{5}	–	5×10^{10}	–
10E	$HSO^-_{3(aq)} \longleftrightarrow H^+_{(aq)} + SO^{2-}_{3(aq)}$	6.22×10^{-8}	3.11×10^{3}	–1960	5×10^{10}	–
11E	$HSO^-_{4(aq)} \longleftrightarrow H^+_{(aq)} + SO^{2-}_{4(aq)}$	1.02×10^{-2}	1.02×10^{9}	–2700	1×10^{11}	–
12E	$HSO^-_{5(aq)} \longleftrightarrow H^+_{(aq)} + SO^{2-}_{5(aq)}$	4.0×10^{-10}	20	–	5×10^{10}	–
13E	$SO_{2(aq)} + H_2O_{(1)} \longleftrightarrow HSO^-_{3(aq)} + H^+_{(aq)}$	3.1×10^{-4}	6.27×10^{4}	–1940	2×10^{8}	–
14E	$FeOH^{2+}_{(aq)} + HSO^{3-}_{3(aq)} \longleftrightarrow FeOHSO_3H^+_{(aq)}$	600	5.0×10^{10}	–	8.3×10^{7}	–
15E	$FeOH^{2+}_{(aq)} + SO^{2-}_{3(aq)} \longleftrightarrow FeOHSO_{3(aq)}$	2.0×10^{7}	5.0×10^{10}	–	2.5×10^{3}	–
16E	$Fe(OH)^{2+}_{(aq)} + H_2O \longleftrightarrow Fe(OH)^+_{2(aq)} + H^+_{(aq)}$	7.0×10^{-5}	5.6×10^{5}	–	8.0×10^{9}	–
17E	$Fe^{2+}_{(aq)} + SO^{2-}_{4(aq)} \longleftrightarrow FeSO_{4(aq)}$	158	7.9×10^{12}	–	5.0×10^{10}	–
18E	$Fe^{3+}_{(aq)} + HSO^-_{3(aq)} \longleftrightarrow FeHSO^{2+}_{3(aq)}$	72	5.0×10^{10}	–	6.9×10^{8}	–
19E	$Fe^{3+}_{(aq)} + SO^{2-}_{3(aq)} \longleftrightarrow FeSO^+_{3(aq)}$	7.3×10^{6}	5.0×10^{10}	–	6.85×10^{3}	–
20E	$Fe^{3+}_{(aq)} + SO^{2-}_{4(aq)} \longleftrightarrow FeSO^+_{4(aq)}$	180	3.2×10^{7}	–	1.8×10^{5}	–
21E	$Fe^{3+}_{(aq)} + H_2O \longleftrightarrow FeOH^{2+}_{(aq)} + H^+_{(aq)}$	0.002	8.6×10^{5}	–	4.3×10^{8}	–

Note: K_i is the equilibrium constant at 298 K; $\vec{A}_{298}$ and $\vec{E}_a$ are the preexponential factor and activation energy of the direct reaction, respectively; and $\overleftarrow{A}_{298}$ and $\overleftarrow{E}_a$ are the preexponential factor and activation energy of the inverse reaction, respectively.

solution containing sulfite. However, its rate is so low that only a small number of the iron ions goes to the solution in the form of Fe(II). However, the catalytic effect of iron ions in the cloud moisture depends on the fraction of dissolved iron and on the distribution of these ions between the Fe(III) and Fe(II) forms. The specificity of atmospheric catalytic sulfite oxidation involving iron ions is evidently associated with the activating effect of UV radiation (and absorption of this radiation) on the droplets of the radical fluxes. For the low concentrations of iron ions[12] ($[Fe]'_{0(aq)} < W_{HO_2^{\cdot}/(Fe)}/J_{39A,\,40A}$), this activation occurs mainly because the radical fluxes (mainly $HO^{\cdot}_{2(g)}$) enter the droplet. Here $W_{HO_2^{\cdot}/(Fe)}$ is the flux of $HO_2^{\cdot}$ radicals in the presence of iron ions in the droplets. Using the above $W_{HO_2^{\cdot}}$ as an approximation, we find $[Fe]'_{0(aq)} \approx 10^{-5}$ mol/l. This means that the substantial activation of catalysis of sulfite oxidation by the iron ions induced by the UV radiation absorption ($FeOH^{2+}_{(aq)}/Fe(OH)^{+}_{2(aq)}$) should only be expected at a rather high $[Fe]_{0(aq)}$. In this case, the partial precipitation of poorly soluble[13] $Fe(OH)_{3(aq)}$, that is, a variable catalyst/substrate ratio in the droplet phase, should also be taken into account. Therefore, below we consider sulfite oxidation catalyzed by the iron ions in the atmosphere for $[Fe]_{0(aq)} \ll [Fe]'_{0(aq)}$.

The accelerating effect of iron ions on sulfite oxidation in the atmosphere is revealed by analysis of the slow step of $SO_{2(g)}$ consumption (see figure). The value of the effect $\Delta\bar{w}\,100\%/\bar{w} = (\bar{w}_{Fe} - \bar{w})100\%/\bar{w}$ at $[Fe]_{0(aq)} = 10^{-7}$ mol/l does not exceed ~15% (here $\bar{w}_{Fe}$ is the time-averaged rate of $SO_{2(g)}$ removal from the gas due to the reactions in the droplet phase containing the iron ions). However, this increase in the sulfite oxidation rate should not be ascribed to the catalytic channel of sulfite oxidation because the mechanism of sulfite consumption radically changes in the presence of the iron ions.

A plot of the sulfite oxidation rate vs. concentration of the iron ions is nonlinear. The dependence of $\bar{w}$ on $[Fe]_{0(aq)}$ is close to a square root function in the interval $10^{-7} \le [Fe]_{0(aq)} \le 4 \times 10^{-7}$ mol/l. This fact disagrees with the results of the scrupulous kinetic study of this reaction under laboratory conditions ($3 \le pH \le 7.5$, $10^{-7} \le [Fe(III)]_{(aq)} \le 10^{-6}$, $10^{-6} \le [S(IV)] \le 2 \times 10^{-5}$ mol/l) [39] suggesting that these processes in a "tube" and in the atmosphere occur via different mechanisms. According to data from [39], the rate of the dark reaction is proportional to the concentration of iron ions, $w_{Fe} = k_{app}^{pH}[Fe]_{0(aq)}[S(IV)]$. Using the experimental value of the apparent rate constant at pH ~ 4 ($k_{app}^{pH4} = 1.7 \times 10^3$ l mol^{-1} s^{-1}), the expected rate constant of sulfur dioxide removal from the gas at $[SO_{2(g)}] \approx 2$ ppbV would be as low as 4×10^{-3} ppbV/h instead of 0.47 ppbV/h (see above).[14] Its still lower value follows from the results presented in [40] and [41] ($k_{app}^{pH4} \approx 10^3$ l mol^{-1} s^{-1}). According to laboratory test data, at such low $[Fe]_{0(aq)}$, the iron ions would be catalytically inactive toward sulfite oxidation. What is the reason for their effect in the atmosphere?

As mentioned above, in the absence of iron ions, the $HO^{\cdot}_{2(aq)}$ radicals decay rapidly in the droplet phase via the reactions $HO^{\cdot}_{2(aq)} + HO^{\cdot}_{2(aq)}/O^{-\cdot}_{2(aq)}$, $HO^{\cdot}_{2(aq)}/O^{-\cdot}_{2(aq)} + SO^{-\cdot}_{5(aq)}$ (1A), (2A), (17A), and (18A) followed by a ~30-fold decrease in $[HO^{\cdot}_{2(g)}]$. In the presence of the iron ions ($[Fe]_{0(aq)} = 10^{-7}$ mol/l), the content of $HO_2^{\cdot}$ in the gas and in the droplets decreases more (~6 times). This decrease is the result of the fast liquid-phase reactions $O^{-\cdot}_{2(aq)} + FeOH^{2+}_{(aq)}/Fe(OH)^{+}_{2(aq)}$ (26A) and (27A), Correspondingly, when $[HO^{\cdot}_{2(aq)}]$ decreases, the rate of the reactions $HO^{\cdot}_{2(aq)}/O^{-\cdot}_{2(aq)} + SO^{-\cdot}_{5(aq)} \longrightarrow HSO^{-}_{5(aq)}$ should decrease. However, the calculations show an increase in the rate of these reactions with an almost unchanged flux to the droplet of the $OH^{\cdot}$ radicals. This increase is related to a dramatic (approximately tenfold) increase in the concentration of the $SO^{-\cdot}_{5(aq)}$ radicals in the presence of iron ions. In the presence of iron ions in the droplet phase, an additional channel of generation of these species appears. The formation of these species is due to the sequence of the liquid-phase reactions:

$$HSO^{-}_{5(aq)} \xrightarrow{Fe^{2+}_{(aq)}} SO^{-\cdot}_{4(aq)} \xrightarrow{HSO^{-}_{3(aq)},\,O_2} SO^{-\cdot}_{5(aq)}.$$

By summing these reactions,

$$FeOH^{2+}_{(aq)} + HO^{\cdot}_{2(aq)} \longrightarrow Fe^{2+}_{(aq)} + H_2O_1 + O_{2(aq)},$$

$$Fe^{2+}_{(aq)} + HSO^{-}_{5(aq)} \longrightarrow FeOH^{2+}_{(aq)} + SO^{-\cdot}_{4(aq)},$$

[12] As we see below, most iron ions exists in the Fe(III) form under the conditions considered. Due to this, $[Fe(III)]_{(aq)} \approx [Fe]_{0(aq)}$.

[13] For example, at pH 5 the maximum concentration of the trivalent iron ions does not exceed ~ $SP_{Fe(OH)_3} K_{16E}K_{21E}[H^+]/K_{3E} \le 2 \times 10^{-7}$ mol/l. Here $SP_{Fe(OH)_{3(aq)}}$ is the solubility product of poorly soluble $Fe(OH)_{3(aq)}$, $SP_{Fe(OH)_3} = 3.8 \times 10^{-38}$ mol^4/l^4 [38].

[14] The w_{Fe} value presented was obtained using the calculated values $[Fe(III)]_{(aq)} \approx 8 \times 10^{-8}$ and $S(IV)_{pH4} \approx [HSO^{-}_{3(aq)}] \approx 4 \times 10^{-7}$ mol/l.

$$SO_{4(aq)}^{-\bullet} + HSO_{3(aq)}^{-} \longrightarrow SO_{3(aq)}^{-\bullet} + H_{(aq)}^{+} + SO_{4(aq)}^{2-},$$

$$SO_{3(aq)}^{-\bullet} + O_{2(aq)} \longrightarrow SO_{5(aq)}^{-\bullet}$$

$$HO_{2(aq)}^{\bullet} + HSO_{3(aq)}^{-} + HSO_{5(aq)}^{-}$$

$$\longrightarrow SO_{4(aq)}^{2-} + H_{(aq)}^{+} + H_2O_{(l)} + SO_{5(aq)}^{-\bullet},$$

we find that the decay of the $HO_{2(aq)}^{\bullet}$ radicals "reducing" the Fe(III) ions in reactions (26A) and (27A) results in the appearance of the "oxidative" $SO_{5(aq)}^{-\bullet}$ radicals in the droplet phase. In the presence of Fe(II), the replacement of the $HO_{2(aq)}^{\bullet}$ radicals by the $SO_{5(aq)}^{-\bullet}$ radicals (so-called "catalytic conversion") when the $OH^{\bullet}$ radical flux to the droplet is virtually unchanged results in an almost tenfold increase in the concentration of the $SO_{5(aq)}^{-\bullet}$ radicals and an increase in the rate of the $HO_{2(aq)}^{\bullet}/O_{2(aq)}^{-\bullet} + SO_{5(aq)}^{-\bullet}$ reactions. The consumption of $HSO_{5(aq)}^{-}$ (30A) in this process (see above) leads to a situation where the $[SO_{5(aq)}^{-\bullet}]$ increase is not accompanied by an increase in $[HSO_{5(aq)}^{-}]$. Thus, the appearance of coupling (with respect to iron(II)) of the reactions $O_{2(aq)}^{-\bullet} + FeOH_{(aq)}^{2+}/Fe(OH)_{2(aq)}^{+}$ (26A), (27A) and $HSO_{5(aq)}^{-\bullet}$ + Fe(II) (30A) under atmospheric conditions is evident. The influence of the coupling of these reactions weakens with an increase in the $SO_{2(g)}$ conversion. This occurs because with a decrease in $SO_{2(g)}$ and, correspondingly, $HSO_{3(aq)}^{-}$ the sulfate radicals react to a greater extent with Fe(II) (33A) instead of $HSO_{3(aq)}^{-}$ (15A). Reaction (33A), being the decay of the reactive species, decreases the rate of replacement of $HO_{2(aq)}^{\bullet} \xrightarrow{Fe} SO_{5(aq)}^{-\bullet}$ and the rate of $SO_{2(g)}$ removal from the gas. This effect manifests itself in the flatter profile of the kinetic curve of $SO_{2(g)}$ consumption at great exposures (see figure, curve for $[Fe]_{0(aq)} = 4 \times 10^{-7}$ mol/l).

At lower $SO_{2(g)}$ conversions in the slow step of its consumption, the increase in the $SO_{5(aq)}^{-\bullet}$ flux due to the "catalytic conversion" $HO_{2(aq)}^{\bullet} \xrightarrow{Fe} SO_{5(aq)}^{-\bullet}$ (calculated per gas) is the following: $\Delta W_{SO_{5(aq)}^{-\bullet}} \approx w_{26A} + w_{27A} \approx 1.3 \times 10^6$ cm^{-3} s^{-1}.[15] This is close to $W_{OH^{\bullet}(Fe)}$ but several (about four) times higher than the sum of the rate of $OH_{(aq)}^{\bullet}$ generation due to the photodissociation of the hydroxo complexes of the iron ions $FeOH_{(aq)}^{2+}/Fe(OH)_{2(aq)}^{+}$ ($[Fe]_{0(aq)} = 10^{-7}$ mol/l) and the liquid-phase reaction $O_{3(aq)} + O_{2(aq)}^{-\bullet}$. Here $W_{OH^{\bullet}(Fe)}$ is the flux of the $OH^{\bullet}$ radicals to the droplet in the presence of the iron ions. Since at $[Fe]_{0(aq)} = 10^{-7}$ mol/l the contributions of the rates of the $SO_{5(aq)}^{-\bullet} + SO_{5(aq)}^{-\bullet}$ and $SO_{5(aq)}^{-\bullet}$ + Fe(II) reactions are rather small (in total, $\leq 4 \times 10^5$ cm^{-3} s^{-1}), $SO_{5(aq)}^{-\bullet}$ is consumed mainly in recombination with the $HO_{2(aq)}^{\bullet}/O_{2(aq)}^{-\bullet}$ radicals. Evidently, their overall rate is $w_{17A} + w_{18A} \approx W_{OH^{\bullet}(Fe)} + \Delta W_{SO_5^{-\bullet}}$. The parallel channel of the $HO_2^{\bullet}$ decrease is its reactions with Fe(III) (26A) and (27A): $\Delta W_{HO_2^{\bullet}} \approx W_{HO_2^{\bullet}(Fe)} - W_{OH^{\bullet}(Fe)} - \Delta W_{SO_5^{-\bullet}}$. This part of the $HO_2^{\bullet}$ radical flux is equal to the increment of the rate of $SO_{5(aq)}^{-\bullet}$ generation due to the "catalytic conversion" $HO_{2(aq)}^{\bullet} \xrightarrow{Fe} SO_{5(aq)}^{-\bullet}$, that is, $\Delta W_{HO_2^{\bullet}} = \Delta W_{SO_{5(aq)}^{-\bullet}}$ and $\Delta W_{SO_{5(aq)}^{-\bullet}} \approx (W_{HO_2^{\bullet}(Fe)} - W_{OH^{\bullet}(Fe)})/2$[16]. Using the calculated values $W_{HO_2^{\bullet}(Fe)}$ and $W_{OH^{\bullet}(Fe)}$, we obtain $\Delta W_{SO_{5(aq)}^{-\bullet}} \approx 1.3 \times 10^6$ cm^{-3} s^{-1}, which agrees with the above increment of the rate of $SO_{5(aq)}^{-\bullet}$ generation.

The consumption of the sulfite in the droplets and, correspondingly, the removal of SO_2 from the gas in the presence of the iron ions occur via two channels. The first channel also occurs in the absence of metal ions. It is related to the formation of $HSO_{5(aq)}^{-}$ ($SO_{5(aq)}^{-\bullet} + HO_{2(aq)}^{\bullet}/O_{2(aq)}^{-\bullet}$) in the droplets followed by the reaction with sulfite (6A). Its rate (taking into account the stoichiometry of (6A)) is evidently $\sim 2w_{6A}$. The additional channel of sulfite consumption ($\sim \Delta W_{SO_{5(aq)}^{-\bullet}}$) results from the replacement of $HO_{2(aq)}^{\bullet} \xrightarrow{Fe} SO_{5(aq)}^{-\bullet}$ in the droplets. In this process the sulfite is consumed by the reaction of $SO_{4(aq)}^{-\bullet}$ with $HSO_{3(aq)}^{-}$ (15A); that is, only one $HSO_{3(aq)}^{-}$ species disappears in the unit cycle of this process. Since $w_{17A} + w_{18A} \approx w_{6A} + \Delta W_{SO_{5(aq)}^{-\bullet}}$, then $w_{17A} + w_{18A} \approx (W_{OH^{\bullet}(Fe)} + W_{HO_2^{\bullet}(Fe)})/2$. Thus, the sum

[15] The rate of the redox cycle of the iron ions is determined by the rates of reactions (26A) and (27A), because the distribution of the charged forms of iron is shifted to Fe(III) under the conditions considered, $\zeta = [Fe(III)]/[Fe(II)] \approx 4$.

[16] In our estimates, $d[SO_{5(aq)}^{-\bullet}]/dt \approx d[HO_{2(aq)}^{\bullet}/O_{2(aq)}^{-\bullet}]/dt \approx d[HSO_{5(aq)}^{-}]/dt \approx 0$.

of these channels of sulfite consumption is $\bar{w}_{Fe} \approx \Delta W_{SO_5^{\cdot-}} + 2((w_{17A} + w_{18A}) - \Delta W_{SO_5^{\cdot-}}) \approx (W_{HO_2^{\cdot}(Fe)} + 3W_{OH^{\cdot}(Fe)})/2$. The calculation of $\bar{w}_{Fe}$ using this equation ($[Fe]_{0(aq)} = 10^{-7}$ mol/l) gives $\bar{w}_{Fe} \approx 3.5 \times 10^6$ cm^{-3} s^{-1} (≈0.5 ppbV/h). Compared with the sulfur dioxide decrease in the absence of iron ions, the increment of the reaction rate is ≈5%. The strict computer calculation of this value gives $(\bar{w}_{Fe} - \bar{w})100/\bar{w} \approx 15\%$. Up to ~40% consumed $SO_{2(g)}$ (instead of 15%, as follows from the simple comparison of $\bar{w}_{Fe}$ and $\bar{w}$) fall on the "catalytic conversion" $HO_{2(aq)}^{\cdot} \xrightarrow{Fe} SO_{5(aq)}^{-\cdot}$.

The expression for $\bar{w}_{Fe}$ does not contain $[Fe]_{0(aq)}$ in explicit form. The influence of iron manifests itself in the fact that the radical fluxes (mainly the $HO_2^{\cdot}$ radical flux) depend on $[Fe]_{0(aq)}$. The calculations show that the increase in $[Fe]_{0(aq)}$ results in an increase in $W_{HO_2^{\cdot}(Fe)}$ and, hence, an increase in the rate of generation of the sulfate radicals, whose amount in reaction (24A) continuously increases. An increase in $W_{HO_2^{\cdot}(Fe)}$ is due to an increase in the rates of reactions (26A) and (27A) in the droplet phase along with a decrease in the concentration of superoxide radicals. The latter results in the enhancement of reactions (23A) and (24A) compared with competing reactions (17A) and (18A). The contribution of reaction (34A) increases simultaneously. The competition of (23A), (24A), and (34A) is the reason for the nonlinearity of the plot of $\bar{w}_{Fe}$ vs. $[Fe]_{0(aq)}$. According to our calculation, the contribution of (23A) and (24A) to the consumption of $SO_{2(g)}$ at $[Fe]_{0(aq)} = 4 \times 10^{-7}$ mol/l is ≈1.6×10^6 cm^{-3} s^{-1} (≈0.2 ppbV/h or the ~30% rate of the $SO_{2(g)}$ decrease).

Taking into account formaldehyde oxidation in the daytime, which is coupled with sulfite oxidation, results in the retardation of $SO_{2(g)}$ removal from the gas phase.[17] This fact is explained by a decrease in the efficiency of the "catalytic conversion" $HO_{2(aq)}^{\cdot} \xrightarrow{Fe} SO_{5(aq)}^{-\cdot}$ induced by the involvement of the sulfate radicals in the reaction $SO_{4(aq)}^{-\cdot} + CH_2(OH)_{2(aq)}$. Its occurrence initiates the chain of consecutive transformations $SO_{4(aq)}^{-\cdot} + CH_2(OH)_{2(aq)} \xrightarrow{O_{2(aq)}} HO_{2(aq)}^{\cdot}/O_{2(aq)}^{-\cdot}$, "returning" the $HO_{2(aq)}^{\cdot}/O_{2(aq)}^{-\cdot}$ radicals, which disappeared in (17A) and (18A). Thus, hydrogen peroxide formation in the droplet phase (1A) and (2A) and its participation in sulfite consumption (3A) are resumed. Correspondingly, sulfite consumption (15A) decreases in parallel with the retardation of the replacement of $HO_{2(aq)}^{\cdot}$ by $SO_{5(aq)}^{-\cdot}$. Finally, this decreases the rate of $SO_{2(g)}$ removal. A similar effect should be expected in the presence of other organic compounds (see [34]). Let us denote the dark catalytic reaction as DCR for sulfite oxidation in the absence of external initiating effects, that is, for the reaction under laboratory conditions. The computer calculation of the Fe(III)/Fe(II) value for the concentration conditions of the slow step of sulfite oxidation in the cloud droplets (pH = 4.0, $[Fe]_{0(aq)} = 10^{-7}$ mol/l and $[S(IV)] = 5 \times 10^{-7}$ mol/l) provided $\zeta_{pH4} = [Fe(III)]/[Fe(II)] \approx 30$ (the Kinetika90 program package). Data from [41] indicate that this calculation is correct. The authors of the cited work experimentally found that $\zeta \approx 6$ for pH 4, $[Fe]_{0(aq)} = 10^{-6}$, and $[S(IV)] = 2 \times 10^{-5}$ mol/l. Our calculation gives $\zeta \approx 7$ for the same conditions.

The limiting unit of the redox cycle for the iron ions in the atmospheric droplets is the reaction of $O_{2(aq)}^{-\cdot}$ with $FeOH_{(aq)}^{2+}/Fe(OH)_{2(aq)}^{+}$. Its characteristic time is determined as $\tau_{26A/27A} = [Fe(III)]_{atm}/\Delta W_{SO_5^{-\cdot}}$. . The limiting unit for the DCR is the decomposition of the Fe(III) sulfite complex (35A), that is, $\tau_{35A} = (k_{35A}\chi)^{-1}$.[18] Comparing these times, we find $\Delta W_{SO_5^{-\cdot}} \times 10^3/k_{35A}\chi[Fe(III)]_{atm}LN_A \le 800$; that is, under atmospheric conditions, the catalytic cycle of sulfite oxidation occurs ~800 times more rapidly! However, this effect is not accompanied by a 800-fold increase in the rate of catalytic sulfite oxidation, which is associated with different stoichiometries of the DCR and atmospheric processes. One catalytic cycle in the DCR oxidizes 18 $HSO_{3(aq)}^{-}$ species [2] because several acts of the reactions $2SO_{5(aq)}^{-\cdot} \longrightarrow 2SO_{4(aq)}^{-\cdot} + O_{2(aq)}$ (24A) and $SO_{4(aq)}^{-\cdot} + HSO_{3(aq)}^{-}$ (15A) occur during the characteristic time of Fe(III) regeneration ($SO_{5(aq)}^{-\cdot}$ + Fe(II) (34A)), and the number of reacted sulfite species is determined as $2(2 + k_{24A}/k_{23A}) = 18$. Under conditions of atmospheric moisture, one catalytic cycle is accompanied by the oxidation of only one sulfite species: reaction (24A) is insignificant against the background

[17] The effect of decreasing the rate of sulfur dioxide removal from the gas due to the reaction between methylene glycol and hydroxyl radicals seems more trivial.

[18]
$$\chi = \frac{K_{14E}[HSO_{3(aq)}^{-}]}{1 + \frac{[H^+]}{K_{21E}} + K_{14E}[HSO_{3(aq)}^{-}] + \frac{K_{16E}}{[H^+]} + \frac{K_{18E}[H^+][HSO_{3(aq)}^{-}]}{K_{21E}} + \frac{K_{10E}K_{19E}[HSO_{3(aq)}^{-}]}{K_{21E}} + \frac{K_{10E}K_{15E}[HSO_{3(aq)}^{-}]}{[H^+]}}.$$

of reactions (17A) and (18A). Thus, the rate of atmospheric sulfite oxidation for the conditions considered is higher than the DCR rate by 44 times and not by 800 times. This striking difference decreases with an increase in the concentration of the iron ions: the rate of cloud sulfite oxidation is proportional to $[Fe]_{0(aq)}^{1/2}$ (see above) and the rate of DCR is proportional to $[Fe]_{0(aq)}$.

It is of interest to present the facts of the qualitative agreement of our calculations of the iron ion distribution with the results of natural measurements. Unfortunately, these data cannot be directly compared because of their intrinsic permanent changes in the concentration conditions, temperature, insolation conditions, and others. For example, in the morning near Zurich (October 18, 1989; 6:00 a.m.–10:00 a.m., $L = (1 - 0.5) \times 10^{-7}$, pH ≈ 5, $[Fe]_{0(aq)} \approx (2–20) \times 10^{-5}$ mol/l, and [S(IV)] ≈ $(1–3) \times 10^{-4}$ mol/l), an increase in the Fe(II) fraction in the droplets, so-called radiation fog, from 0.5 at 6:00 a.m. to 0.9 at 10:00 a.m., was detected [42]. In this period of the insolation increase, the concentrations of $OH_{(g)}^{\bullet}$ and $HO_{2(g)}^{\bullet}$ and their fluxes to the droplet increase and reactions (26A) and (27A) are accelerated. In parallel with this process, an increase in the insolation intensity results in the acceleration of Fe(II) formation during the $FeOH_{(aq)}^{2+}/Fe(OH)_{2(aq)}^{+}$ dissociation. On the other hand, under conditions of orographic cloud [16] at $[Fe]_{0(aq)} = (2–3) \times 10^{-7}$ mol/l, the concentration of the Fe(II) ions turned out to be lower than the sensitivity of the analytical method. These measurements were carried out at a very low illumination and correspondingly low $[OH_{(g)}^{\bullet}]$ and $[HO_{2(g)}^{\bullet}]$.

In the calculations of the "complete" model of "remote atmosphere" [12], the fraction of the Fe(II) ions is close to unity ($[Fe]_{0(aq)} = 5 \times 10^{-7}$ mol/l, $[SO_{2(g)}]_0$ = 1 ppbV, $[Cl_{(aq)}^{-}] = 10^{-4}$ mol/l). The rate of the sulfur dioxide decrease due to the liquid-phase reactions was $\sim 2 \times 10^6$ cm^{-3} s^{-1}. According to our calculations, ignoring the reactions of the chloride ions ($[SO_{2(g)}]$ = 3 ppbV, $[Fe]_{0(aq)} = 4 \times 10^{-7}$ mol/l), sulfur dioxide decreases with a rate of $\sim 5 \times 10^6$ cm^{-3} s^{-1}. This discrepancy is nonrandom. It is induced by the suppression of the "catalytic conversion" $HO_{2(aq)}^{\bullet} \xrightarrow{Fe} SO_{5(aq)}^{-\bullet}$ by the chloride ions. Their interaction with the sulfate radicals $SO_{4(aq)}^{-\bullet} + Cl_{(aq)}^{\bullet} \longrightarrow SO_{4(aq)}^{2-} + Cl_{(aq)}^{\bullet}$ results in several reversible reactions: $Cl_{(aq)}^{\bullet} + Cl_{(aq)}^{-} \rightleftharpoons Cl_{2(aq)}^{-\bullet}$, $Cl_{(aq)}^{\bullet} + H_2O_{(l)} \rightleftharpoons ClOH_{2(aq)}^{-\bullet} + H_{(aq)}^{+}$; $ClOH_{(aq)}^{-\bullet} \rightleftharpoons Cl_{(aq)}^{-} + OH_{(aq)}^{\bullet}$, and $ClOH_{(aq)}^{-\bullet} + Cl_{(aq)}^{-} \rightleftharpoons Cl_{2(aq)}^{-\bullet} + OH_{(aq)}^{-}$ [12]. Taking into account these reactions makes it possible to present the cycle of transformations describing the catalytic conversion of $HO_{2(aq)}^{\bullet}$ to $OH_{(aq)}^{\bullet}$

$$FeOH_{(aq)}^{2+} + HO_{2(aq)}^{\bullet} \longrightarrow Fe_{(aq)}^{2+} + H_2O_{(l)} + O_{2(aq)},$$

$$Fe_{(aq)}^{2+} + HSO_{5(aq)}^{-} \longrightarrow FeOH_{(aq)}^{2+} + SO_{4(aq)}^{-\bullet},$$

$$SO_{4(aq)}^{-\bullet} + Cl_{(aq)}^{-} \longrightarrow SO_{4(aq)}^{2-} + Cl_{(aq)}^{\bullet},$$

$$Cl_{(aq)}^{\bullet} + H_2O_{(l)} \longrightarrow ClOH_{(aq)}^{-\bullet} + H_{aq}^{+},$$

$$ClOH_{(aq)}^{-\bullet} \longrightarrow Cl_{(aq)}^{-} + OH_{(aq)}^{\bullet},$$

$$HO_{2(aq)}^{\bullet} + HSO_{5(aq)}^{-} \longrightarrow SO_{4(aq)}^{2-} + H_{(aq)}^{+} + OH_{(aq)}^{\bullet} + O_{2(aq)}.$$

The calculation shows that the rate of catalytic conversion $HO_{2(aq)}^{\bullet} \xrightarrow{Fe} OH_{(aq)}^{\bullet}$ at $[Cl_{(aq)}^{-}] = 10^{-4}$ mol/l ($\sim 1.9 \times 10^6$ cm^{-3} s^{-1}) is so high that the droplet becomes the emitter of $OH_{(g)}^{\bullet}$ into the gas phase. This problem for different $[Fe]_{0(aq)}$, $[SO_{2(g)}]$, and others will be examined elsewhere.

ACKNOWLEDGMENTS

This work was supported by the Russian Foundation for Basic Research (project nos. 01-02-16172 and 00-05-64029).

REFERENCES

1. Yermakov, A.N. and Purmal, A.P., *Program and Abstr., Fourth Int. Conf. on Chemical Kinetics*, Gaithersburg, 1997, p. 283.
2. Yermakov, A.N. and Purmal, A.P., *Global Atmospheric Change and Its Impact on Regional Air Quality*, Barnes, I., Ed., New York: Kluwer Academic, 2000, p. 163.
3. Ermakov, A.N. and Purmal', A.P., *Kinet. Katal.*, 2001, vol. 42, no. 4, p. 531.
4. Wilson, C. and Hirst, D.M., *Prog. React. Kinet.*, 1996, vol. 21, p. 69.
5. Ermakov, A.N. and Purmal', A.P., *Kinet. Katal.*, 2002, vol. 43, no. 2, p. 273.
6. Ermakov, A.N., Larin, I.K., Purmal', A.P., *et al., Khim. Fiz.*, 2002, vol. 19, no. 4, p. 61.
7. Segneur, C. and Saxena, P., *Atmos. Environ., A*, 1984, vol. 18, p. 2109.
8. Graedel, T.E., Mandich, M.L., and Wescheler, C.J., *J. Geophys. Res.*, 1986, vol. 91, p. 5205.
9. Gery, M.W., Whitten, G.Z., Killus, J.P., *et al., J. Geophys. Res.*, 1989, vol. 94, p. 12925.
10. Matthijsen, J., Builtjes, P.J.H., and Sedlak, D.L., *Meteor. Atmos. Phys*, 1995, vol. 57, p. 43.
11. Karol', I.L., Zatevakhin, M.A., Ozhigina, N.A., *et al., Izv. Akad. Nauk, Fiz. Atmos. Okeana*, 2000, vol. 36, p. 778.
12. Herrmann, H., Ervens, B., Jacobi, H.-W., *et al., J. Atmos. Chem.*, 2000, vol. 36, p. 231.
13. Jacob, D.J., *J. Geophys. Res.*, 1986, vol. 91, p. 9807.

14. Jacob, D.J., Gottlieb, E.W., and Prather, M.J., *J. Geophys. Res.*, 1989, vol. 94, p. 12975.
15. Langner, J. and Rodhe, H., *J. Atmos. Chem.*, 1991, vol. 13, p. 255.
16. Sedlak, D., Hoigne, J., David, M.M., *et al.*, *Atmos. Environ.*, 1997, vol. 31, no. 16, p. 2515.
17. Schwartz, S.E. and Freiberg, J.E., *Atmos. Environ., A*, 1981, vol. 15, p. 1129.
18. Schwartz, S.E., *Chemistry of Multiphase Atmospheric Systems.*, Jaeschke, W., Ed., Berlin: Springer, vol. 6, p. 415.
19. Seinfeld, J.H. and Pandis, S.N., *Atmospheric Chemistry and Physics. From Air Pollution to Climate Change*, New York: Wiley, 1998, p. 1326.
20. *Chemical Workbench*, http://www.kintech.ru.
21. JPL publication, 1997.
22. http://www.iupac-kinetic.ch.cam.ac.uk.
23. Larin, I.K. and Ugarov, A.A., *Khim. Fiz.*, 2002, vol. 19, (in press).
24. Yermakov, A.N., Zhitomirskii, D.M., Poskrebyshev, G.A., *et al.*, *J. Phys. Chem.*, 1993, vol. 97, p. 10712.
25. Marsh, C. and Edwards, J.O., *Prog. React. Kinet.*, 1989, vol. 15, p. 35.
26. Das, T.N., *J. Phys. Chem.*, 2001, vol. 105, p. 9142.
27. Betterton, E.A. and Hoffman, M.R., *J. Phys. Chem.*, 1988, vol. 92, p. 5962.
28. McElroy, W.J. and Deister, U., National Power Research Report. ESTB, *L/0173/R90*, 1990.
29. Elias, H., Götz, U., and Wannowius, K.J., *Atmos. Environ., A*, 1994, vol. 28, p. 439.
30. Herrmann, H., Jacobi, H.-W., Reese, A., *et al.*, *Fresenius' J. Anal. Chem.*, 1996, no. 355, p. 343.
31. Travina, O.A., Ermakov, A.N., Kozlov, Yu.N., *et al.*, *Kinet. Katal.*, (in press).
32. Barlow, S., Buxton, G.V., Salmon, G.A., *et al.*, *EUROTRAC Ann. Rep.*, 1993, part 6, p. 48.
33. Calvert, J.G. and Stockwell, W.R., *Acid Precipitation Series*, Calvert, J.G., Ed., Boston: Butterworth, 1984, vol. 3, p. 1.
34. Isdorov, V.A., *Organicheskaya khimiya atmosfery* (Organic Chemistry of Atmosphere), Leningrad: Khimiya, 1985, p. 265.
35. Jacob, D. and Hoffman, M.R., *SO_2, NO, and NO_2 Oxidation Mechanisms: Atmospheric Consideration*, Calvert, J.G., Ed., 1984, part 3, p. 101.
36. Hoffmann, H., Hoffmann, P., and Lieser, K.Y., *Fresenius' J. Anal. Chem.*, 1991, vol. 340, p. 591.
37. Grgić, I., Hudnick, V., Bizjak, M., *et al.*, *Atmos. Environ., A*, 1992, vol. 27, p. 1409.
38. Alekseev, V.N., *Kolichestvennyi analiz* (Quantitative Analysis), Moscow: Goskhimizdat, 1954, p. 474.
39. Ibusuki, T. and Takeuchi, K., *Atmos. Environ., A*, 1987, vol. 21, p. 1555.
40. Grgić, I., Hudnick, V., Bizjak, M., *et al.*, *Atmos. Environ., A*, 1991, vol. 25, p. 1591.
41. Sedlak, D.L. and Hoigné, J., *Environ. Sci. Technol.*, 1994, vol. 28, p. 1898.
42. Behra, P. and Sigg., L., *Nature*, 1990, vol. 344, p. 419.